Identification, Classification and Mapping of Surface Soil Types Using Hyperspectral Remote Sensing Datasets

Amol D. Vibhute*[1], Karbhari V. Kale[2], Rajesh K. Dhumal[1], Ajay D. Nagne[1], Suresh C. Mehrotra[2]

*[1]Geospatial Technology Research laboratory, Department of Computer Science & IT,

Dr. Babasaheb Ambedkar Marathwada University, Aurangabad, Maharashtra, India.

amolvibhute2011@gmail.com*[1]

[2]Department of Computer Science & IT, Dr. Babasaheb Ambedkar Marathwada University, Aurangabad,

Maharashtra, India.

ABSTRACT

The traditional methods of soil analysis are tedious and they do not fulfill the rapid requirements of spatiotemporal variability. The present study highlights the use of hyperspectral remote sensing (HRS) datasets for soil classification. The Minimum Noise Fraction (MNF) method was implemented for dimensionality reduction of huge Hyperion data. First, ten MNFs were provided precious information. The Analytical Spectral Device (ASD) non-imaging spectroradiometer was used for recording the collected 74 soil samples. The reference spectra was analyzed and used for Hyperion image classification. The Spectral Angle Mapper (SAM) method was computed after dimensionality reduction by MNF method for soil classification. The overall accuracy of SAM classifier was 91.77 percent with Kappa Value 0.89. The black cotton soil, lateritic soil and sand dunes of surface soil types were identified, classified and mapped. The outcome of the present study is essential for digital soil analysis and its mapping of heterogeneous area.

Keywords: Soil Classification, Hyperspectral Data, Soil Properties, Soil Types Identification, Soil Taxonomy, Minimum Noise Fraction, Spectral Angle Mapper, Dimensionality Reduction, Accuracy Assessment.

I. INTRODUCTION

Soil is one of the most important resources and vital component of earth's critical zone. There are extraordinary pressures on soil due to urbanization, industrialization or from degradation; soils are reducing their quality that are unbalancing the agricultural practices and food production. Consequently, soil quality and its management with planning are essential to preserve the soil with its quality for future generations [1]. In addition, soil mapping plays a vital role in planning, management of landform and soil use for sustainable growth of the area. Accordingly, identification, classification of surface soil types along with its mapping is mostly an imperative task for agricultural practices like crop growth and condition monitoring and worldwide food production. However, globally soils are very heterogeneous and dynamic in environment as compared to air and water which structure, study and processes are also complicated and formidable both spatially and temporally [2], [3]. Moreover, the spatiotemporal variability of soils does not fulfilled by the conventional laboratory methods. Furthermore, soil analysis and its mapping by conventional laboratory methods are time consuming, tedious and expensive [4]. Recently, HRS datasets (both imaging and non-imaging) has provided

tremendous information about earth surface materials for identifying minute details of various materials on the earth surface especially soils with high spectral and spatial resolution data [5]. Consequently, identification, classification and mapping of surface soil types through HRS datasets are constructive tool for better agricultural and land planning with its management [6].

Under HRS conditions, an effort has been made to identify the surface soil types for classification and its mapping by digital ways. The background of the soil analysis via customary procedures and recent advancements with HRS technology of it is illustrated in section first. Section two depicts the details of studied region. The used HRS datasets are given in section three. The proposed methodology for analysis of soils are revealed in section four. Section five discusses the obtained results by proposed approach. Conclusions of the present study are drawn in section six.

II. THE STUDY AREA

The Kanhori, Pal, Wanegaon and Pimpalgaon Walan village parts, agricultural sectors and hilly region of Aurangabad district of Maharashtra, India were chosen as the study area for the current research. The geographical location of the study area (Figure 1) is situated at 19°28'43.27"- 20°24'52.19" N latitude and 75°13'10.75" -75°30'14.87" E longitude (20° 06' N latitude and 75°25' E longitude).
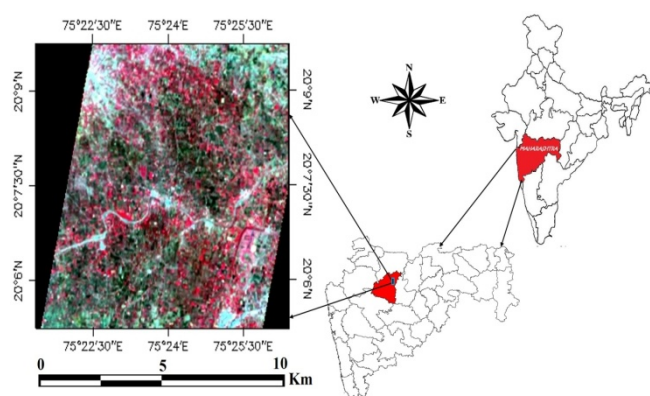
Figure 1. The Geographical Location of the Study Area

The total size of the study area is near about 62.35 Km^2 which has heterogeneous in nature with hilly regions and surrounded by Aurangabad Taluka at South, Sillod Taluka at East and Khultabad and Kannad Taluka at West [7]. The study site has semiarid atmosphere at an elevation of near about 580 meters above the sea level. An annual usual rainfall is near about of 710mm with an annual average temperature is 17° C to 33° C. The surface soil type of the site is black cotton soil and cotton, maize and bajra are the major crops.

III. THE USED HYPERSPECTRAL DATASETS

3.1 EO-1 Hyperion Hyperspectral Data

USGS with NASA have launched EO-1 satellite for acquiring the images of earth surface features from continuous very narrower wave channels by its Hyperion sensor. The Hyperion data was obtained by USGS [8] on 15 April 2015, at 17:15 hrs, which was over passed at the studied site on 20 March 2015. The obtained Hyperion image was radiometrically and geometrically (orthorectified) (Level 1T) corrected by the provider which was band sequential (BSQ) files having 0 to 9% cloud cover. The data has 242 spectral channels with 10 nm spectral resolution and 30m spatial resolution with 7.75 km by 100 km swath per scene. The data covers spectral channels of wavelength range from 355.59-2577.08 nm. The VNIR range consists of 400-1000nm spectral range along with SWIR range is 900-2500nm through a push-broom mode. The level 1T product has 242 spectral channels among those 1-70 channels for VNIR and 71-242 channels for SWIR. Accordingly, final L1T product provides 198 channels having radiometric calibration parameters. The total 198 channels represents 426.82-2395.5 nm continuous spectrum with Full Width at Half the Maximum (FWHM) 10-nm. Only 196 channels were unique due to overlap between the VNIR and SWIR focal planes [9], [10]. The position of each field site (ground truth points) was gained from a real-time GPS and digital camera of Sony Experia Smartphone.

3.2 Soil Sampling and its Spectra Acquisition

The topsoil (0-20cm depth) soil samples were collected from the agricultural parts of the studied area during the period of 10 February-25 March 2015 in between 0800 to 1330 hrs in airtight containers. The soil sampling was performed with their snapshots and their geolocation values of GPS were collected in near-real time to coincide with satellite sensor overpass. The soil sampling was carried out with clear climate just after the harvest of cotton, wheat and Jawar crops. The surface crop/plant relics were removed by hands while collecting the samples in airtight containers. The total number of 74 samples was collected, air-dried, and passed through 2mm sieve for laboratory analysis. The soil properties were analyzed by standard laboratory methods at "MIT Soil and Water Testing Laboratory", Aurangabad, Maharashtra, India.

The spectra of the collected soil samples were acquired by ASD Field Spec 4 spectroradiometer [11] for obtaining the reflectance spectra of soils. The ASD provides the reflectance spectra at VNIR-SWIR wavelengths ranging from 350-2500nm, yielding the total of 2151 spectral values per spectrum. The spectral measurements were instantly taken after the soil samples collection from the agricultural sites. The device has high spectral resolution with 3nm for 350-1000nm and 10nm for 1000-2500nm along with sampling interval 1.4nm and 2nm for each range. The soil samples were placed at the bottom of a 20cm diameter with 2cm thickness Petri dish using a high intensity source probe. The 75w tungsten quartz halogen filament lamp as an illumination source for illuminating the soil samples was used. The lamp was set as 60° of Zenith angle at a distance of 45cm above the soil sample. The reflected light was collected in 1-nm bandwidths between 350-2500nm with an 8° FOV fiber-optic cable of spectroradiometer that was kept off-nadir at a distance of 15 cm above the soil samples. The instrument was optimized and calibrated using white reference panel and then samples were recorded [12]. The average of 10 spectra of each sample was recorded to minimize the noise produced by the instrument for obtaining the final spectra. The RS3 (Version 6.3) inbuilt software was used to record the reflected spectra. The acquired non-imaging raw spectra of soils were imported in View Spec Pro (6.0.11) software for averaging the similar spectra and renovated it. The renovated spectra were latterly imported into ENVI software as reference spectra (with reference pixels) for training the HRS imaging data which was used for classification and generation of thematic map.

IV. THE PROPOSED METHODOLOGY

The following methodology was implemented in ENVI (Environment for Visualizing Images) 5.1 Hyperspectral image analysis package and ARC GIS 10 software for data processing. The workflow of proposed methodology is depicted in Figure 2 and proposed overall methodology consists of following steps:

1. Conversion of Hyperion hyperspectral image which was in the form of level 1T GeoTIFF into ENVI standard format using 'Hyperion tools toolkit'.
2. Removal of uncalibrated and water vapour channels.
3. Renovation of digital number (DN) values to Radiance Value.
4. Atmospheric correction by QUAC algorithm and radiance to reflectance with generation of False Colour Composite (FCC) image RGB-VNIR (R-51, G-30, B-20).
5. Spatial and spectral subset of the test site.
6. Dimensionality reduction by MNF and first ten MNFs were considered to preserve 98 percent of the variance generation which were used for classification.
7. The collected soil samples were analyzed with laboratory methods for getting the physicochemical properties of soils and soil reflectance spectra were analyzed and used as training set for image classification.

8. The Hyperion image pixels were selected rely on the developed reference spectra of soil samples collected by ASD device along with collected ground reference data from field visit.

9. The validation or testing pixels were selected using ROI tool for Hyperion data by ground truth.

10. Executed SAM algorithm using Equation 2.

11. Accuracy assessment using confusion matrix and kappa coefficient by ROIs.
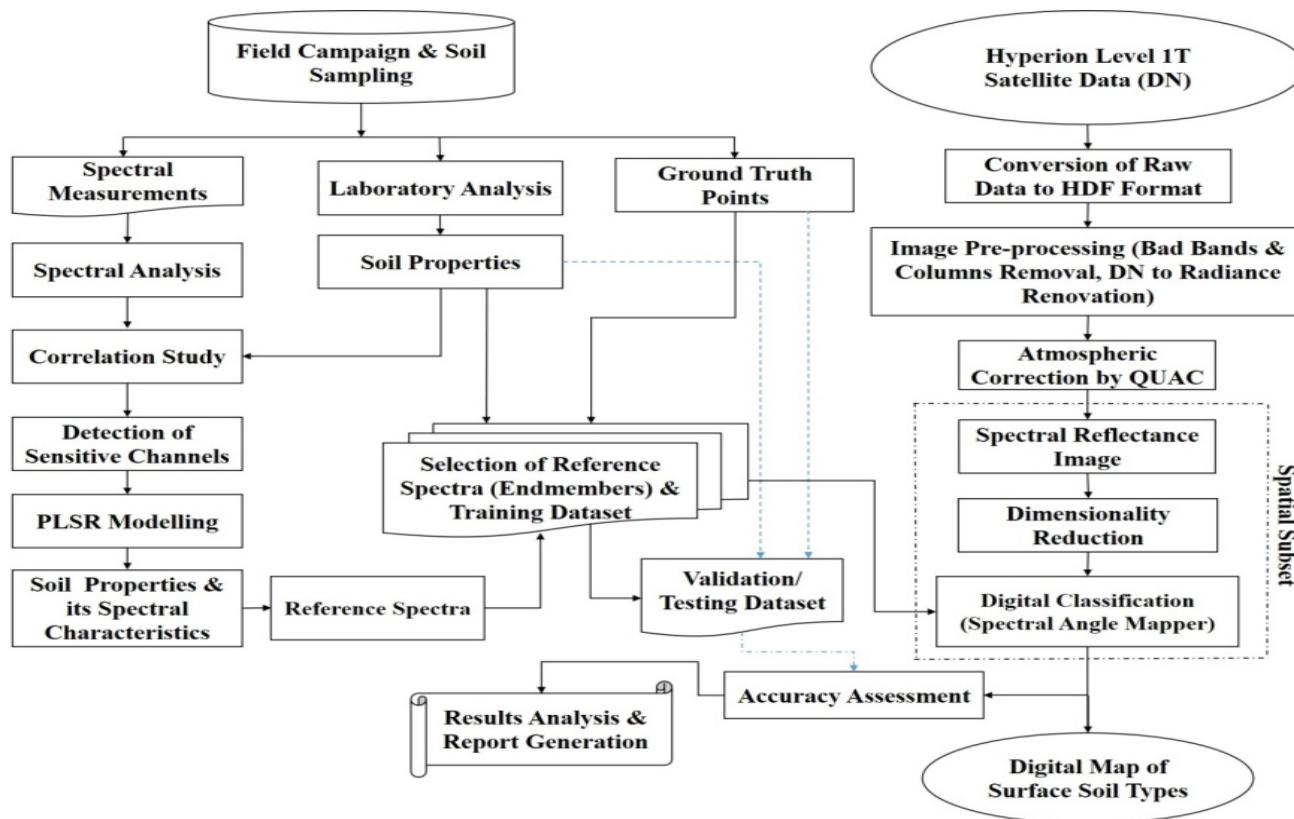
Figure 2. Workflow of Proposed Methodology

4.1 Spectral Analysis of Non-Imaging Hyperspectral data

Firstly, the collected soil samples were analysed by the standard laboratory methods for getting its physicochemical properties. Similarly, the spectra of soil samples were acquired and analysed for obtaining pure reference spectra of soils. The correlation study was carried out on the basis of soil properties obtained by laboratory reports. Sensitive channels were detected and Partial Least Squares Regression (PLSR) based regression method was computed to predict the soil properties from non-imaging spectra. The soil properties and its spectral characteristics were analysed and validated to develop reference spectra. The developed pure reference spectra were used for training the Hyperion imagery for classification.

4.2 HRS image Pre-Processing
4.2.1 Elimination of Water Vapour and Uncalibrated Channels:

The water vapour and uncalibrated channels were detected and eliminated from the further processing. The obtained level 1T product were having 242 channels among that, channels 1-70 were for VNIR and 71-242 were for SWIR region of spectrum. Channels 1-7, 58-70, 71-76 and 225-242 were not calibrated and set to zero during level 1B pre-processing. Remaining VNIR 8-57 and SWIR 77-224 channels were calibrated. Hence, total 198 channels were calibrated with VNIR 56, 57 and SWIR 77, 78 channels. The overlapping channels 77 and 78 channels having low Signal-to-Noise-Ratio (SNR) value, hence eliminated to gain 196 unique channels [9], [10].

On the other hand, strongest water vapour channels were detected in between 120-132, 165-182, 185-187 and 221-224 and eliminated from the processing [9], [10]. Consequently, remaining 155 channels are useful for further processing as eliminated channels 1-7, 58-78, 80-82, 120-132, 165-182, 185-187, 221-242. The calibrated 155 channels have valuable information about the earth surface, which provides the prime input channel set for further processing and image interpretation. After eliminating uncalibrated and water vapour channels, the stable subset of remaining 155 key channels with their spectral wavelengths is listed in the Table 1.

TABLE 1. HYPERION HYPERSPECTRAL 155-CHANNELS AFTER CHANNEL REMOVAL

Hyperion Channel Name	Hyperion Channels	Spectral Wavelengths (nm)
VNIR	8-57	426.82-925.41
SWIR	79	932.64
SWIR	83-119	972-1336
SWIR	133-164	1477.43-1790.18
SWIR	183-184	1981.85-1991.95
SWIR	188-220	2032.35-2355.20

4.2.2 Conversion of DN values to Radiance:
Furthermore, the 155 key channels were renovated for getting the radiance values by two scaling factors i.e. 40 for VNIR (1-70) channels and 80 for SWIR (71-242) channels. VNIR (1-70) channels and SWIR (71-242) channels individually were divided by these scaling factors 40 and 80 respectively [9], [10].

4.2.3 Atmospheric correction using QUAC Algorithm:
The QUAC algorithm is used for atmospheric correction due to its empirical approach which allows radiance values of a view for the removal of atmospheric effects. Moreover, the QUAC algorithm works better without any ancillary metadata. Additionally, the radiance values were converted into visible reflectance values.

Consequently, the reflected 155 calibrated channels of Hyperion imagery were kept for additional processing and QUAC atmospheric algorithm were

implemented on it [10] due to atmospheric issues. The QUAC [13] was implemented using Equation 1.

$$\rho = (\rho_1 + \rho_2 + ... + \rho_n)/n \qquad 1$$

where, ρ are the end member spectrum of the surface and the average reflectance of different materials, and n specifies the end member number.

4.3 Dimensionality Reduction of Hyperion Data

The huge dimensionality of Hyperion data was reduced by dimensionality reduction methods. Hyperspectral satellite data which is having number of spectral channels of a similar view causes the computational burden, obscurity and time. Hughes demonstrated that, with increased number of features or dimensionality of data in spectral domain may affect adversely the classification accuracy or leads to poorer classification [14]. Accordingly, MNF method was implemented on atmospherically corrected Hyperion imagery to reduce the huge dimensionality.

4.3.1 Minimum Noise Fraction (MNF):
The MNF method is a linear transformation modified with principal component (PC) transform developed by Green [15] in 1988 to abolish or filter the noisy channels from the images moreover to detract the hyperspectral dimensionality. The PC transform does not construct components with a steadily increasing noise level when the availability of differing amounts of noisy channels which causes critical to pick a cut-off point. Ergo, MNF method has been popular than PC transform which accomplish a components dataset that does have increasing noise (diminishing signal-to-noise) as an substitute to principal component analysis (PCA) method. Two rotations of PCA are followed in MNF. Firstly, the PCs of the noise covariance matrix is decorrelated and rescaled the noisy data (noise whitening), resulting in transformed data in which the noise has unit variance and no band-to-band correlations. Secondly, the PCs derived from the original image datasets after noise-whitened data. MNF is essentially used to determine the inherent dimensionality of image data,

to segregate noise in the data, and to diminish the computational necessities for subsequent processing. The MNF method divides the data into two sections. The section first produces the huge eigenvalues coupled with coherent eigenimages. The second section generates the near-unity eigenvalues and noise-dominated images. Using merely the coherent portions splits the noise from the datasets, accordingly improving spectral processing results [15].

MNF method was also computed on atmospherically corrected Hyperion dataset and computed appropriate MNF features from it. The Table 2 indicates the resulted eigenvalues, cumulative percentage and percentage variation using MNF method.

TABLE 2. EIGEN VALUES, CUMULATIVE PERCENTAGE AND VARIABILITY OF PERCENTAGE OF FIRST 10 MNFS

MNF	Eigen values	Eigen values in Percentage	Cumulative Percentage	Variability of Percentage
$\lambda 1$	183.480	26.21	55.15	55.15
$\lambda 2$	81.5384	37.85	79.66	24.50
$\lambda 3$	15.2277	40.03	84.23	4.57
$\lambda 4$	11.0271	41.60	87.55	3.314
$\lambda 5$	8.5989	42.83	90.13	2.584
$\lambda 6$	8.2192	44.00	92.60	2.47
$\lambda 7$	7.6224	45.09	94.89	2.29
$\lambda 8$	5.8885	45.93	96.66	1.77
$\lambda 9$	5.6895	46.75	98.37	1.71
$\lambda 10$	5.3915	47.52	100	1.62

4.4 Hyperspectral Image Classification by SAM Method

SAM is a physically based spectral classification method is widely popular in hyperspectral image classification while using an n-D angle to match the image pixels to the reference spectra or spectral library. The SAM method determines the spectral similarity between two spectra by calculating the spectral angle between the spectra and treating them as vectors in a space with dimensionality equal to the number of channels [16]. The SAM method is comparatively insensitive to the illumination and albedo effects, when used on calibrated reflectance spectra. It considers each pixel in the image and estimates the similarity of the spectra. The input for SAM method is an endmember spectra can come from ASCII files or developed spectral libraries, or extracted spectra from the image directly by ROIs. The angle between reference spectra and image pixels are matched with smaller angle represents closer matches. Those pixels are more away from the specified maximum angle threshold in radians are not considered for classification. SAM classification assumes reflectance data. Nevertheless, if radiance data is used, the error is generally not significant because the origin is still near zero [16]. Mathematically, the SAM method was implemented by Equation 2.

$$\alpha = \cos^{-1}\left(\frac{\sum_{i=1}^{nb} t_i r_i}{\left(\sum_{i=1}^{nb} t^2_i\right)^{1/2} \left(\sum_{i=1}^{nb} r^2_i\right)^{1/2}} \right) \qquad 2$$

where, t is the test spectrum, r is the reference spectrum and nb is the number of channels. More theory with its illustration of angle between reference spectrum and test spectrum will be found at reference in detail [16].

4.5 Classification Accuracy Assessment

Finally, the implemented SAM method was evaluated for accuracy of Hyperion data. The producer's accuracy, user's accuracy, overall accuracy with kappa coefficient was examined by ground truth points for accuracy assessment. The confusion matrix was generated from ground truth points. Confusion matrix can be used to determine a classified label against actual ground observation at specified location. The nondiagonal nonzero value indicates the error between the classified objects from corresponding observation [17]. The classification accuracy was assessed with producer's accuracy, user's accuracy, overall accuracy along with kappa coefficient and it was calculated through Equation 3, 4, 5 and 6 respectively [18], [19].

$$\text{Producer's accuracy} = \frac{C_{xx}}{\sum_r} \times 100\% \qquad 3$$

where, C_{xx} is the element at position x^{th} row and x^{th} column and $\sum_r$ is row sums.

$$\text{User's accuracy} = \frac{C_{yy}}{\sum_c} \times 100\% \qquad 4$$

where, $\sum_c$ is column sums.

$$\text{Overall accuracy} = \frac{\sum_{x=1}^{A} C_{xx}}{N} \times 100\% \qquad 5$$

where, N and A is the total number of pixels and classes respectively.

$$k = \frac{\sum_{i=1}^{r}(X_{ii} - \sum_{ci}\sum_{ri})}{N^2 - \sum_{i=1}^{r}(\sum_{ci}\sum_{ri})} \qquad 6$$

where, r=number of rows and columns in the error matrix, X_{ii}=number of observations in row i and column i, $\sum_{ci}$=marginal total of column i, $\sum_{ri}$ = marginal total of row i, N=total number of observations.

V. RESULTS AND DISCUSSION

5.1 Hyperion Data Pre-processing
The Hyperion image was illustrated using FCC for better visual interpretation. The resampling method was Nearest Neighbour and datum was WGS-84 rectified by UTM zone 43 North. The spatial subset was generated using ROIs. After spatial subset the original image (1011 x 3481 pixels) was resized with 293 x 277 pixels which was our study region and from where soil samples were collected. The coordinates of the study area for upper left was 200945.47 N and 752122.44 E, where as lower right was 200514.54 N and 752624.19 E.

5.2 The MNF Method Outcomes
MNF method was implemented for dimensionality reduction as the outcome (Table 2) was evaluated on the basis of Eigen values and visual interpretation of obtained MNFs. The illustrated outcomes of first ten

MNFs are drawn in Figure 3. It was observed by the eigenvalues and its cumulative percentage, first ten MNFs were more spectral information. Thus, merely first ten channels were used for further processing and remaining channels were ignored from the computation. The Table 2 clearly shows the obtained information by the MNF method with first ten MNFs. Consequently, only first ten MNFs were valuable spectral information which was used for endmembers (pure pixels of soils) extraction. The obtained first ten MNFs are illustrated in Figure 3, which contained more spectral information with less variance and MNF 3, 6 and 7 were not having the noise as they illustrated good. It was observed that, the noises present in the images were segregated in the higher number MNF channels and it was point out that there is a decrease in spatial coherency with increasing MNF channel number. The transformed MNF imagery was used for classification of soils.
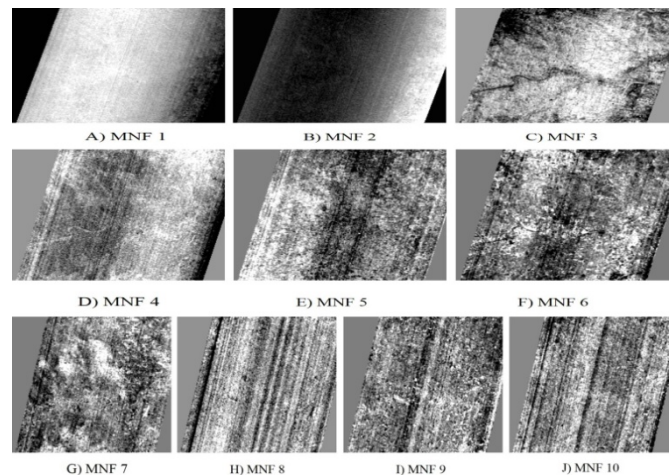
Figure 3. First Ten MNFs of 155 Channels of Hyperion Image

5.3 Soil Types Identification and Laboratory Reports
According to laboratory analysis of soil physicochemical properties, reference spectra of soil types generated by ASD on the basis of spectral signature characteristic (correlated with the laboratory results), and MNF spectral features, one major (black cotton soil or 'Regur') and two minor (Lateritic soil and Sand dunes) soil types were identified and classified with other two land features. The black cotton soil [20] includes vertisol, inceptisol

and entisol, where as lateritic soil includes alfisol soil. Sand dunes include arenosols or typic torripsamments. Furthermore, the identified soil classes such as black cotton soil, lateritic soil, sand dunes along with vegetations and settlements were considered and classified.

The image spectra were compared with field spectra for each soil surface feature. The spectral features of soils were extracted on the basis of spectral signature characteristic of non-imaging reflectance spectra, laboratory physicochemical analysis of soil properties, geolocated ground reference data, and visual inspection of soil colours and are compared with HRS imaging data. The Hyperion data with SAM classification method was trained rely on the field observations in the combinations with laboratory analysis and the spectral characteristics of geolocated non-imaging data. The developed reference spectra of soil types by non-imaging device along with ground truth points were used for training the Hyperion image. The ROIs were developed by said reference points which were used for the SAM based classification to test the Hyperspectral imagery for classification.

According to USDA soil taxonomy [21], [22] five soil classes were detected and classified on the basis of report generated by the said methods and imaging reflectance spectra. The soil classes were vertisol, inceptisol and entisol of black cotton soil, alfisol of lateritic soil, arenosols or typic torripsamments of sand dunes. Additionally, other two earth surface features were considered such as vegetations and settlements due to high availability of it.

The spectra of soil features were distinguished accordingly the spectral reflectance properties within the specified spectrum range. The soil physicochemical properties like soil water (moisture) contents, soil organic matter, soil Fe contents and soil clay contents are main factors to decrease the spectral reflectance of soils [23], [24]. However, the absorption peaks of water (moisture and hydroxyl ions) were found at 1400-1450 nm and 1900-1950 nm [25].

5.4 The SAM Method Reports of Soil Classification

The SAM method was implemented using the Equation 2 for the classification of Hyperion image. The spectral hyper-angle is calculated between each pixel and target spectra. Spectral endmembers (Rules images) were produced using 0.15 radians value angle for matching the reference spectra of soil (derived by ASD) for the unknown image spectra and the Hyperion image classification was obtained using all spectra of the surface features concurrently for the SAM method. The SAM method provides the radians value to each class individually. Here, all classes have given 0.15 radians values except settlement due to fewer pixels of it. The digital map of surface soil types were mapped using SAM with MNF method. The resulted soil classification map is shown in Figure 4. The classified map clearly shows that, there were most regions were covered by the black cotton soil of the studied area. It was observed that, black cotton soil is the dominant soil of the study area [20], [26] followed by alfisol soil of lateritic group. Sand dunes, vegetations and settlements were classified well using SAM in the combination of MNF. The classification map (Figure 4) clearly indicate that, black cotton soils [22] have covered most area of the test site followed by sand dunes (arenosols or typic torripsamments), lateritic (alfisols) soil, vegetations and settlements.

As per the laboratory reports of soils, these black soils are deep or heavy and medium or lighter as per its physical properties. The textures of black soils are loamy to clayey with mixed carbonates (mostly $CaCo_3$) and are suitable for cotton cultivation [20]. The soil organic carbon, soil organic matter and nitrogen found to be less in this soil and pH values are near about 7-9. The Electrical Conductivity (EC) values vary from 0.25 and 0.46 d Sm-1 where values were less than 0.36 d Sm-1. The iron contents are good in black soils. According to USDA soil taxonomy [21] the black soils are vertisol, inceptisol

and entisol. The lateritic soil included only the alfisol in the studied areas as per USDA soil taxonomy which found to be hilly part and somewhat farming sectors of test site.
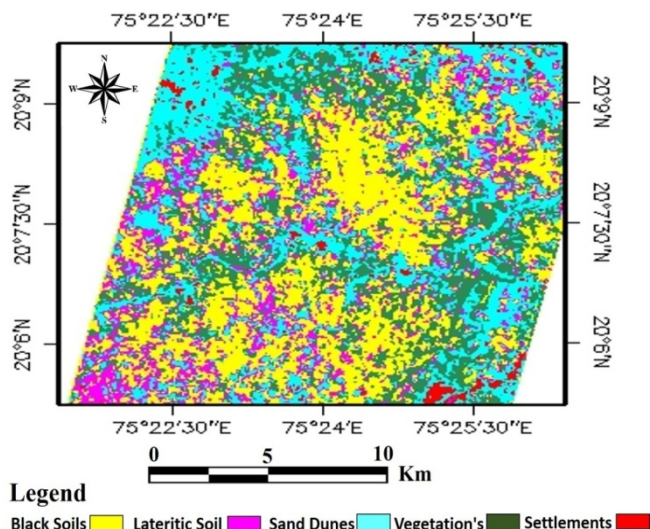
Figure 4. Classification Map of Surface Soils using SAM with MNF method

The pH value of these soils a low and organic matter is high with fine texture. Sand dunes were observed to be more at riverside and hilly rocks due to the spectral structure of sand dunes and rocks. Sand dunes [27] are having coarse sandy texture that does not hold the water and nutrient storage capacity is low and high permeability that does not useful for farming practices. However, dry farming practices can be possible with sand dunes using sufficient fertilizers where annual rainfall exceeds 300nm. The EC values and organic matter contents are very low in sand dunes. Sand dunes are categorized as 'Arenosols' [27] accordingly World Reference Base for Soil Resources and 'Typic Torripsamments' [21] accordingly USDA soil taxonomy. Natural vegetations including agricultural crops were accurately classified and mapped. There were minor misclassification between sand dunes and settlements due to spectral similarity of these two classes.

5.5 Accuracy Assessment of Classification

Lastly, the confusion matrix was generated using reference spectra of soils with ground control points for estimating the classification accuracy of soil features. The confusion matrix along with classification accuracy of various classes of soils and two other classes using SAM and MNF methods are located in Table 3. The total number of 304 ground control points was used for accuracy assessment. The classification accuracy was assessed with producer's accuracy, user's accuracy, overall accuracy and kappa value and are calculated though Equation 3, 4, 5 and 6 respectively. The error of commission and error of omission [18] were also calculated for all classes indicated in Table 3.

TABLE 3. CONFUSION MATRIX OF CLASSIFICATION DERIVED BY SAM METHOD (MNF) AND ACCURACY ASSESSMENT

Classes	Soil Reference Data and Ground Data (Pixels)					
	BCS	**LS**	**SD**	**Veg**	**Set**	**RT**
BCS	**82**	8	0	0	0	90
LS	0	**58**	0	0	0	58
SD	0	1	**24**	0	0	25
Veg	0	0	0	**64**	0	64
Set	0	1	15	0	**51**	67
CT	82	68	39	64	51	**304**
PA (%)	100	85.29	61.54	100	100	
UA (%)	91.11	100	96.00	100	76.12	
CE (%)	8.89	0.00	4.00	0.00	23.88	
OE (%)	0.00	14.71	38.46	0.00	0.00	
Overall Accuracy= **91.77** (279/304), Kappa Value= **0.89**						

Where, BCS-Black Cotton Soil, LS-Lateritic Soil, SD-Sand Dunes, Veg-Vegetations, Set-Settlements, RT-Row Total, CT-Column Total, PA-Producers Accuracy, UA-Users Accuracy, CE-Commission Error and OE-Omission Error.

The overall classification accuracy was achieved 91.77 percent with kappa values of 0.89 for SAM with MNF method. The diagonal values of the confusion matrix (Table 3) indicate the correctly classified pixels into their classes. In fact, all the classes were classified accurately as our objective was to detect and classify surface soil types which were classified well. The class-specific accuracies, black cotton soil, lateritic soil and vegetations were classified with the superior accuracy excluding sand dunes which were misclassified with settlements due to assorted similarity of spectral signature characteristics. The reflectance of sand dunes and settlements were observed to be very close spectral signature characteristics and thus misclassified to each other and yielded lower accuracies. The Table 3 clearly depicts that, there were misclassifications between sand dunes with settlements classes due to said reasons.

VI. CONCLUSIONS

The HRS datasets plays a vital role in identification, classification and mapping of the surface soil types with satisfactory outcomes. The laboratory analysis of soil physicochemical properties and obtained outcome of non-imaging remote sensing data were used as a reference (input) for imaging datasets to identify and classify the surface soil types. The essential pre-processing of hyperspectral imaging data were carried out which includes noise or uncalibrated channels removal, bad columns removal, radiance to reflectance conversion with atmospheric correction. The major contribution of the present research is to develop reference spectra of soil types and soil classification scheme. The soil classification was done accordingly USDA soil taxonomy. The outcome of the present research is proved the use of non-imaging spectra is crucial for SAM method to identify and classify the surface soil types. The MNF method provided good results for dimensionality reduction of Hyperion data. It is concluded that, the SAM method is suitable for soil type's classification with good accuracy. The developed map of soil surface types with its analysis of properties can be effectively used in precision farming, land planning, management and decision making for various applications.

VII. ACKNOWLEDGEMENTS

VIII. REFERENCES

[1]. Rossel, R. V., Behrens, T., Ben-Dor, E., Brown, D. J., Demattê, J. A. M., Shepherd, K. D., ... & Aïchi, H. (2016). A global spectral library to characterize the world's soil. Earth-Science Reviews, 155, 198-230.

[2]. Rossel, R. V., Walvoort, D. J. J., McBratney, A. B., Janik, L. J., & Skjemstad, J. O. (2006). Visible, near infrared, mid infrared or combined diffuse reflectance spectroscopy for simultaneous assessment of various soil properties. Geoderma, 131(1), 59-75.

[3]. Anne, N. J., Abd-Elrahman, A. H., Lewis, D. B., & Hewitt, N. A. (2014). Modeling soil parameters using hyperspectral image reflectance in subtropical coastal wetlands.

International Journal of Applied Earth Observation and Geoinformation, 33, 47-56.

[4]. Vibhute, A.D., Gawali, B.W. (2013). Analysis and modeling of agricultural land use using remote sensing and geographic information system: a review. Int. J. Eng. Res. Appl. (IJERA,) 3(3), 081–091.

[5]. Ben-Dor, E., Patkin, K., Banin, A., & Karnieli, A. (2002). Mapping of several soil properties using DAIS-7915 hyperspectral scanner data-a case study over clayey soils in Israel. International Journal of Remote Sensing, 23(6), 1043-1062.

[6]. Vibhute, A. D., Kale, K. V., Dhumal, R. K., & Mehrotra, S. C. (2015, December). Soil type classification and mapping using hyperspectral remote sensing data. In Man and Machine Interfacing (MAMI), 2015 International Conference on (pp. 1-4). IEEE.

[7]. http://www.onefivenine.com/india/villages/Aurangabad-District/Phulambri/Kanhori.

[8]. http://earthexplorer.usgs.gov/.

[9]. Beck, R., (2003). EO-1 User Guide Version 2.3. Satellite Systems Branch, USGS Earth Resources Observation Systems Data Center (EDC).

[10]. Vibhute, A. D., Kale, K. V., Dhumal, R. K., & Mehrotra, S. C., (2015). Hyperspectral Imaging Data Atmospheric Correction Challenges and Solutions using QUAC and FLAASH Algorithms. IEEE, International Conference on Man and Machine Interfacing (MAMI), 1-6.

[11]. https://www.asdi.com/.

[12]. Hatchell, D. C. (1999). Analytical Spectral Devices. Inc. (ASD) Technical Guide.

[13]. Guo, Y., & Zeng, F., (2012). Atmospheric Correction Comparison of Spot-5 Image Based On Model FLAASH and Model QUAC. International Archives of the Photogrammetry, Remote Sensing and Spatial Information Sciences, XXXIX-B7, 7-11.

[14]. Hughes, G. (1968). On the mean accuracy of statistical pattern recognizers. IEEE transactions on information theory, 14(1), 55-63.

[15]. Green, R. O., Eastwood, M. L., Sarture, C. M., Chrien, T. G., Aronsson, M., Chippendale, B. J., ... & Olah, M. R. (1998). Imaging spectroscopy and the airborne visible/infrared imaging spectrometer (AVIRIS). Remote sensing of environment, 65(3), 227-248.

[16]. Kruse, F. A., Lefkoff, A. B., Boardman, J. W., Heidebrecht, K. B., Shapiro, A. T., Barloon, P. J., & Goetz, A. F. H. (1993, August). The spectral image processing system (SIPS) -interactive visualization and analysis of imaging spectrometer data. In AIP Conference Proceedings (Vol. 283, No. 1, pp. 192-201). AIP.

[17]. Vibhute, A. D., Nagne, A. D., Gawali, B. W., & Mehrotra, S. C. (2013). Comparative analysis of different supervised classification techniques for spatial land use/land cover pattern mapping using RS and GIS. Int. J. Sci. Eng. Res, 4(7), 1938-1946.

[18]. Gao, J. (2009). Digital analysis of remotely sensed imagery. McGraw-Hill Professional.

[19]. Vibhute, A. D., Dhumal, R. K., Nagne, A. D., Rajendra, Y. D., Kale, K. V., & Mehrotra, S. C. (2016). Analysis, Classification, and Estimation of Pattern for Land of Aurangabad Region Using High-Resolution Satellite Image. In Proceedings of the Second International Conference on Computer and Communication Technologies (pp. 413-427). Springer, New Delhi.

[20]. Basu, P. K. (2011). Methods manual: soil testing in India. Department of Agriculture & Cooperation, Ministry of Agriculture Government of India New Delhi. Krishi Bhawan, New Delhi, 110001.

[21]. USDA (2014). Keys to Soil Taxonomy, United States Department of Agriculture. Natural Resources Conservation Service.

[22]. Bhattacharyya, T., Pal, D. K., Mandal, C., Chandran, P., Ray, S. K., Sarkar, D., ... & Sahoo, A. K. (2013). Soils of India: historical

perspective, classification and recent advances. Current Science, 1308-1323.

[23]. Bilgili, A. V., Van Es, H. M., Akbas, F., Durak, A., & Hively, W. D. (2010). Visible-near infrared reflectance spectroscopy for assessment of soil properties in a semi-arid area of Turkey. Journal of Arid Environments, 74(2), 229-238.

[24]. Chang, C. W., Laird, D. A., Mausbach, M. J., & Hurburgh, C. R. (2001). Near-infrared reflectance spectroscopy–principal components regression analyses of soil properties. Soil Science Society of America Journal, 65(2), 480-490.

[25]. Reeves, J., McCarty, G., & Mimmo, T. (2002). The potential of diffuse reflectance spectroscopy for the determination of carbon inventories in soils. Environmental pollution, 116, S277-S284.

[26]. U.S. Balpande (2013). Ground Water Information Aurangabad District Maharashtra, Central Region Nagpur. Govt of India Ministry of Water Resources Central Ground Water Board.

[27]. IUSS Working Group WRB. 2015. World Reference Base for Soil Resources 2014, update 2015 International soil classification system for naming soils and creating legends for soil maps. World Soil Resources Reports No. 106. FAO, Rome.